

Development of a Quasi-Steady Flow Electrochemical Paper-Based Analytical Device

Jaclyn A. Adkins, Eka Noviana, and Charles S. Henry

Anal. Chem., **Just Accepted Manuscript** • DOI: 10.1021/acs.analchem.6b03010 • Publication Date (Web): 26 Sep 2016

Downloaded from <http://pubs.acs.org> on September 27, 2016

Just Accepted

“Just Accepted” manuscripts have been peer-reviewed and accepted for publication. They are posted online prior to technical editing, formatting for publication and author proofing. The American Chemical Society provides “Just Accepted” as a free service to the research community to expedite the dissemination of scientific material as soon as possible after acceptance. “Just Accepted” manuscripts appear in full in PDF format accompanied by an HTML abstract. “Just Accepted” manuscripts have been fully peer reviewed, but should not be considered the official version of record. They are accessible to all readers and citable by the Digital Object Identifier (DOI®). “Just Accepted” is an optional service offered to authors. Therefore, the “Just Accepted” Web site may not include all articles that will be published in the journal. After a manuscript is technically edited and formatted, it will be removed from the “Just Accepted” Web site and published as an ASAP article. Note that technical editing may introduce minor changes to the manuscript text and/or graphics which could affect content, and all legal disclaimers and ethical guidelines that apply to the journal pertain. ACS cannot be held responsible for errors or consequences arising from the use of information contained in these “Just Accepted” manuscripts.



Development of a Quasi-Steady Flow Electrochemical Paper-Based Analytical DeviceJaclyn A. Adkins,[†] Eka Noviana,[†] and Charles S. Henry*[†][†]Department of Chemistry, Colorado State University, Fort Collins, Colorado 80523, United States*E-mail: Chuck.Henry@colostate.edu. Phone: +1-970-491-2852.1
2
3
4
5
6
7
8
9
10
11
12
13
14
15
16
17
18
19
20
21
22
23
24
25
26
27
28
29
30
31
32
33
34
35
36
37
38
39
40
41
42
43
44
45
46
47
48
49
50
51
52
53
54
55
56
57
58
59
60

Abstract

An electrochemical paper-based analytical device (ePAD) was developed for quasi-steady flow detection at microwire electrodes, for the first time. The device implements a fan shaped geometry connected to an analysis channel whereby solution is pulled from an inlet, through a channel, and into the steadily increasing capillary network of the fan. The network counteracts the decrease in solution flow rate associated with increasing viscosity within the channel, generating quasi-steady flow within the analysis channel. Microwire electrodes were embedded between two paper layers within the analysis channel, such that solution flow occurred on both sides of the wire electrodes. The quasi-steady flow ePAD increased the current by 2.5 times and 0.7 times from a saturated channel with no flow and from a single-layer paper device with flow respectively. Amperometric detection was used for flow injection analysis (FIA) of multiple analytes at both Au and Pt microwire working electrodes, both of which provided similar sensitivity (*ca.* 0.2 mM⁻¹) when normalized to the same standard. The two-layer paper devices provided a detection limit of 31 μM for p-aminophenol (PAP) using Pt electrodes and was also used to detect enzyme activity for the reaction of β-Galactosidase with p-aminophenyl-galactopyranoside (PAPG). Measured enzyme kinetics provided similar V_{max} (0.079 mM / min) and K_m (0.36 mM) values as those found in the literature. This device shows great promise towards use in enzyme-linked immunosorbent assays or other analytical techniques where flow or washing steps are necessary. The developed sensor provides a simple and inexpensive device capable of performing multiple injection analysis with steady-flow and on-line detection that would normally require an external pump to perform.

Introduction

The development of microfluidic devices in combination with lab-on-a-chip technologies has offered platforms that are inexpensive, with minimal reagent use, waste generation and analysis time. Furthermore, they are often simpler to use than traditional benchtop instrumentation.¹ Many microfluidic devices have also been designed with the intention of point-of-need measurements away from the traditional laboratory setting. While many microfluidic devices have been demonstrated in the laboratory, few have been adapted to point-of-need measurements.² One reason for this lack of product acceptance is that many devices require external pumps and tubing for continuous flow, making them inconvenient for field measurements. Paper has long been used as a platform for analytical measurements and more recently in microfluidic devices since Whitesides *et al.* published the use of photoresist-patterned filter paper for the multiplexed biomarker detection.³ Since then, a variety of methods for device fabrication and analyte detection in microfluidic paper-based analytical devices (μPADs) have been developed.⁴⁻⁶ The popularity of using paper as a substrate for analytical analysis lies in its inherent advantage of being an inexpensive, disposable, and easy to modify platform that contains a capillary network capable of fluid transport and manipulation without the need for external pumps.^{7,8} These advantages also make μPADs well suited for point-of-care (POC) and environmental analysis where demand for low-cost and simple to use devices that can contain stored reagents is high.^{6,9,10}

While colorimetric detection has been the most common detection method for μPADs due to its simple reactions and easily visible results, electrochemical paper-based analytical devices (ePADs), as first proposed by Dungchai *et al.*¹¹ can provide lower detection limits and generate more quantitative results when compared with colorimetric detection.¹² Detection electronics can also be miniaturized and battery powered for portable and simple detection of multiple analytes (i.e. a handheld glucose

meter).¹³ Although many ePADs have been developed to perform detection in quiescent solution, few have been developed for detection in flow. Flow in paper devices is driven by capillary force,¹⁴ gravity,¹⁵ and/or pressure differences from an inlet and outlet.¹⁶ While these systems have been used effectively, ePADs developed for flow injection analysis (FIA) are less common.¹⁷ FIA has the advantage of being able to detect multiple sample additions with time, for example, Dossi *et al.* presented a system for FIA detection at pencil drawn electrodes in a paper-based channel.¹⁷ Solution was pulled through the channel by an attached wicking pad, and this system showed good repeatability and reproducibility for up to seven measurements. However, to the best of our knowledge no other ePADs have demonstrated the steady-state flow in combination with FIA detection.

Several methods for electrode fabrication and incorporation into ePAD devices have been developed.^{18,19} The most common method involves using a screen¹¹ or stencil²⁰ to pattern conductive carbon or metallic inks onto paper. Carbon has been the most common ePAD electrode material, due to its low-cost, widespread availability, and wide potential window for detection.¹⁸ Metallic electrodes, however, have also been used, and provide their own unique advantages including; higher conductivity and alternative catalytic activity and subsequent electrochemistry from carbon. Metal electrodes, most commonly gold and silver, have been deposited onto the surface of paper using thin film deposition techniques,²¹ nanoparticle growth,^{22,23} or inkjet printing.²⁴ Similar to previous work presented by our group in which microwires were incorporated into polymer microfluidic devices,²⁵ microwires have also been incorporated into paper-based devices. Crooks and coworkers first published the use of microwire electrodes within paper devices.²⁶ These prefabricated electrodes could be easily cleaned and modified prior to incorporation into an ePAD and without damaging the paper substrate. Previous work by our group further studied the use of microwires in contact with paper and found that they provided higher flux of species to the electrode surface and improved electrochemical performance from paper-based electrodes reported in the literature and fabricated carbon ink electrodes.^{27,28} Although microwire electrodes have been incorporated into ePAD devices,^{26,28} these devices employed quiescent solutions.

Herein, we report the first use of microwire electrodes in a paper-based flow-through device. The device integrates a unique geometry adapted from a previously reported device concept by Mendez *et al.*²⁹ Originally proposed as a method to create a steady solution flow for lateral flow assays, the developed device makes use of a regularly increasing capillary network in the shape of a 270° fan connected to an inlet channel. This fan geometry is used to compensate for the decay in flow rate within the analysis channel that coincides with the distance a fluid front travels through a capillary network (Lucas-Washburn Law).³⁰⁻³² However, to the best of our knowledge this device design has never been implemented with any analyte detection motif aside from dye-based flow characterization. The fan design generates a steady flow of solution through an inlet channel and the integration of electrodes within this channel offers the possibility to detect multiple samples with time and without a decay in fluid transport that would also result in a decay in mass transport to the electrode and resulting in a decay in measured current. Additionally, the use of a sandwiched paper format on both sides of the microwire electrodes allows for full immersion of the electrode in a flow through ePAD, increasing the available electrode working area. As proof of concept, an enzyme kinetics study was conducted with the device to determine time-based reaction variables using β -Galactosidase and *p*-aminophenyl-galactopyranoside (PAPG) as enzyme and substrate respectively. This reaction generates *p*-aminophenol (PAP) which is a common product in electrochemical immunoassays as well as a health indicator or contaminant in clinical and environmental samples respectively, due to its use or byproduct production

1
2
3 in pesticides, dyes, and pharmaceuticals.³³ As such, PAP serves as a model analyte for broader
4 applications.
5
6
7

8 Experimental Section

9 **Materials.** Potassium chloride (KCl), potassium nitrate (KNO₃), potassium hydroxide (KOH), iron (III)
10 chloride hexahydrate (FeCl₃·6H₂O), potassium ferricyanide (K₃Fe(CN)₆), 30% hydrogen peroxide (H₂O₂),
11 and Whatman #1 filter paper were purchased from Fisher Scientific (Fairlawn, NJ). Benzoquinone (BQ)
12 and p-aminophenol (PAP) were purchased from Alfa Aesar (Ward Hill, MA) and EMD Millipore (Billerica,
13 MA) respectively. Hydroquinone (HQ), β-galactosidase enzyme and p-aminophenyl-galactopyranoside
14 (PAPG) substrate were purchased from Sigma-Aldrich. Both enzyme, substrate, and stock solution
15 aliquots were stored at -20°C prior to use. Fresh aliquots were thawed prior to use daily. Potassium
16 ferrocyanide (K₄Fe(CN)₆) was purchased from Mallinckrodt Chemical Works (St. Louis, MO). High-purity
17 silver ink was purchased from SPI Supplies (West Chester, PA). Electrode materials, 99.99% pure gold
18 (25 μm) and platinum (30 μm) microwires (diameter), were purchased from California Fine Wire
19 Company (Grover Beach, CA). All reagents were used as received without further purification. All
20 electrochemical measurements were done using either an eDAQ EA161 Potentiostat and EC201 e-
21 Corder (Denistone East, Australia) or a CHI 660B Electrochemical Workstation (Austin, TX). 2-in-wide
22 Scotch® brand heavy duty clear shipping packaging tape was purchased from 3M (St. Paul, MN). Devices
23 were printed using a Xerox (Norwalk, CT) ColorCube 8870 wax printer and stencils, paper and tape
24 components were cut using a 30 W Epilog (Golden, CO) Zing Laser Cutter and Engraver.
25
26
27

28
29 **Microwire ePAD Fabrication.** Similar to previously described work, ePADs were designed using
30 CorelDRAW (Corel, Ottawa, Ontario), a graphic design program, and fabricated on Whatman #1 filter
31 paper.²⁸ Fluid flow and containment were achieved by printing hydrophobic wax barriers using a wax
32 printer. Wax printed designs of 4-pt line thickness were melted through the filter paper on a 150 °C
33 hotplate for 90 s to create wax barriers. Packing tape was used to seal the bottom of the device and
34 prevent leaking. On the printed side, microwires were spaced 1 mm apart across the channel device
35 using printed alignment marks as guides and either taped in place with a packing tape cover or covered
36 with a laser-cut Whatman wicking layer, followed by the laser-cut packing tape cover (Scheme 1A and B).
37 The paper-based sample inlet used a 6-mm diameter (4.1-mm inner diameter after melting) wax printed
38 well connected to a channel that is 11-mm long by 5-mm wide (11.2-mm length by 3.1-mm inner width
39 after melting). The channel flows into the center of a 30-mm diameter circle (27.8-mm inner diameter
40 after melting) with a 90° section removed to form a 270° wicking fan from the channel end. The laser-
41 cut wicking top of the device has the same dimensions as the paper region bound by the melted wax
42 described in parenthesis above. The laser-cut packing tape cover consists of a rectangle (9-mm x 7-mm)
43 connected 8-mm into a 34-mm diameter circle. The packing tape cover is made so that the tape covers
44 approximately 1-mm past the wax printed and melted outer edge of the device to create a protective
45 seal and hold the microwire electrodes and wicking layer in place on top of the wax printed layer of the
46 device. The sample well inlet is left uncovered for sample addition. Silver paint was applied to wire ends
47 to create touchpads that could be connected to the potentiostat (Scheme 1C).
48
49
50

51
52 **Characterization of Device with Flow.** Visual determination and color analysis software were used to
53 characterize flow within single and double-paper layer devices. The Lucas-Washburn flow behavior
54 within straight channels with single and double-layers of paper were characterized visually by dipping
55 the sample inlet into a dye solution and measuring the height of the fluid front with time. The channels
56 were fabricated with the same sample inlet and channel width dimensions as the quasi-steady flow
57 device described above, but with a channel length extended to 90 cm (Supplemental Figure S1). Steady
58
59
60

1
2
3 flow behavior was measured within the ePAD device made with either a single layer of paper or double
4 layer by measuring the increase in colored area with time from photos using ImageJ analysis software.
5 ImageJ was used to isolate the red region formed within the device and measure the normalized growth
6 in area until the device was completely red within the wax defined region.
7
8

9 Device flow was also characterized using amperometry by the repeated addition of 5 or 10 μL of a blank
10 injection consisting of 0.5 M KCl, or a sample containing 5 mM $\text{K}_4\text{Fe}(\text{CN})_6/\text{K}_3\text{Fe}(\text{CN})_6$ in 0.5 M KCl to the
11 sample inlet. Electrochemical detection was determined using Au or Pt microwire electrodes. The
12 average current was measured from the steady-state flow and resulting steady-state current produced.
13 Linear-sweep voltammetry (LSV) was taken of 5 mM $\text{K}_4\text{Fe}(\text{CN})_6/\text{K}_3\text{Fe}(\text{CN})_6$ in 0.5 M KCl at Au microwire
14 electrodes, in a saturated paper-based channel or while solution was flowing within the ePAD device.
15 The saturated channel containing electrodes were made by removing the fan shaped region at the end
16 of the channel and adding solution ($\sim 20 \mu\text{L}$) to the inlet until no more solution was removed from the
17 inlet to wick down the channel.
18
19

20
21 **Flow ePAD Calibration.** Calibration detection of flow devices was carried out using amperometry with
22 droplet addition as described above for repeatability experiments. 5 or 10 μL droplets of solution were
23 added to the device and the average plateau current was plotted against concentration, for both Pt and
24 Au working electrodes and with either $\text{K}_4\text{Fe}(\text{CN})_6/\text{K}_3\text{Fe}(\text{CN})_6$ or HQ/BQ in 0.5 M KCl, or PAP in pH 7.4
25 laboratory-prepared phosphate buffered saline (PBS, 8.00 g NaCl, 0.24 g KCl, 1.44 g of Na_2HPO_4 , and
26 0.24 g KH_2PO_4 , per liter of distilled water). Plateau currents were then normalized to a standard added at
27 the end of each use and plotted against concentration to create a normalized calibration curve.
28 Standards were 5 mM $\text{K}_4\text{Fe}(\text{CN})_6/\text{K}_3\text{Fe}(\text{CN})_6$ and HQ/BQ for the same species calibration curves and 1
29 mM $\text{K}_4\text{Fe}(\text{CN})_6/\text{K}_3\text{Fe}(\text{CN})_6$ in 0.5 M KCl for PAP calibration.
30
31

32 **Enzyme Kinetics Detection.** The ePADs were used to perform a kinetic study on β -galactosidase activity
33 using 4-aminophenyl β -D-galactopyranoside (PAPG) as the substrate. The product of this enzymatic
34 reaction, *p*-aminophenol (PAP), is a redox active molecule. The flow device design contained one Pt
35 microwire reference electrode and two Pt microwires working and two platinum counter electrodes.
36 Cyclic voltammograms (CVs) of 1 mM PAPG or 1 mM PAP in pH 7.4 PBS were acquired at 0.1 V/s from
37 0.2 to 0.7 V vs Pt and from -0.1 to 0.4 V vs Pt, respectively to study electrochemical properties of both
38 species. The optimal applied over-potential for PAP detection from the PAPG background current was
39 determined by detecting the plateau current with droplet flow through the device using amperometry
40 at 0.1, 0.2, 0.3, and 0.4 V vs Pt. A 0.3 V optimal applied over-potential was determined and employed for
41 the duration of amperometric measurements for PAP detection. A PAP calibration curve was established
42 by measuring 0-1 mM PAP solutions in pH 7.40 PBS. To ensure reproducibility of enzymatic detection
43 within the devices, three separate 100 μL solutions containing 1 mM PAPG and 5 U/mL beta-
44 galactosidase were prepared in fresh pH 7.40 PBS before analysis and were added in 5 μL aliquots to
45 separate devices every 60-100 seconds until the measured current reached a plateau. Similarly, to
46 obtain the rate of reaction at different concentrations of substrate, equal volumes of 10 U/mL beta-
47 galactosidase solution and 0.2-10 mM PAPG solutions were mixed (end concentration of 5 U/ml and 0.1-
48 5 mM PAPG), and the current was measured during the initial linear enzymatic response. At least five
49 time points were collected for each substrate concentration to calculate the rate of reaction from the
50 linear slope obtained from change in current with time. Current was converted to PAP concentration
51 using the previously obtained PAP calibration curve. Measurements were done in three separate devices
52 and the measured rates for each device were averaged. A Lineweaver-Burk plot (i.e. $1/[\text{substrate}]$ vs
53 $1/\text{rate}$ plot) was established and the Michaelis-Menten constant (K_m) was extracted from the plot.³⁴
54
55
56
57
58
59
60

Results and Discussion

Device Design Theory. Aside from the low-cost, a key advantage to using paper as an analytical platform lies in exploiting the capillary force generated from the hydrophilic network of cellulose fibers to imbibe solution into the device. Both lateral flow assays and many paper-based devices take advantage of this passive flow to implement sample mixing, reaction timing and washing steps that would otherwise necessitate the use of external pumps and pipetting steps.⁴ However, a disadvantage to using paper is that flow velocity decreases with time within capillaries of constant cross-sectional area (such as in lateral flow assays and paper-based channels). When considering sensor response, this decay can increase the assay time as well as change detection response as a function of time. While the capillary driving force itself remains constant within a channel of constant cross sectional area, there is an increase in viscous drag force due to the increase in wetted area and the distance the fluid front moves from the inlet reservoir. This behavior is described by the Lucas-Washburn equation:³¹

$$l(t) = \sqrt{\left(\frac{\gamma r \cos \theta}{2\mu}\right) t} \quad (1)$$

where the distance the fluid front travels with time ($l(t)$) is directly proportional to the square root of time (t), cosine of the solution contact angle with paper (θ), solution surface tension (γ) and the mean capillary pore radius or effective pore radius of the paper (r), as well as indirectly proportional to the square root of the viscosity (μ).³¹ Figure 1A shows the experimentally measured increase in fluid front distance within a straight channel for both one- and two-layer devices (device images shown in Supplemental Figure S1). As previously observed by Camplisson *et al.*, a noticeable increase in flow rate is achieved when using two layers of paper to imbibe solution within a channel.³⁵ This increase was attributed to an increase in the effective pore radius, due to the gap between the sheets acting as a larger capillary. They experimentally determined an increase from 0.11 μm (average pore radius within Whatman #1 filter paper) for imbibition in a single layer of paper to 0.34 μm , due to the inclusion of the gap between the two layers of paper.

While the prior work determined the average pore radius with evaporative variables, the device design employed in this work uses tape to seal the device, thus minimizing evaporation. Using Equation 1 to fit the experimental data with solution terms for water at room temperature ($\gamma = 0.0728 \text{ N}\cdot\text{s}/\text{m}^2$), and $\theta = 0$ for Whatman #1 filter paper, the effective pore radius was calculated to be 0.15 ± 0.01 and $0.38 \pm 0.06 \mu\text{m}$ for one- and two-layer devices respectively. The slightly larger effective pore radius is probably due to the addition of tape acting as another capillary wall, where it is not adhered to the fibers and serving to keep solution and humidity within the device. The calculated gap height between the paper layers, using a weighted average of the calculated effective pore radius values (Equation S1),³⁵ was determined to be 12 μm , which is reasonable given the visual spacing shown in cross-sections as discussed below and matches the reported value obtained by Camplisson *et al.*³⁵

One way to overcome the increase in viscous drag force and therefore decay in flow rate was proposed by Mendez *et al.*²⁹ This relies on a steady increase in the fluid front area in the shape of a 270° fan attached to the channel exit, providing a counterbalance to the capillary pressure. The flow behavior for the fully wetted capillary network within the channel can be described by Darcy's Law.³⁶

$$Q = \frac{\kappa w h P_c}{\mu L} \quad (2)$$

1
2
3 where the volumetric flow rate (Q) is directly proportional to the capillary pressure ($P_c=2\gamma \cos \theta / r$),
4 interstitial permeability (κ , approximated to be $r^2/8$), channel width ($w = 3.1$ mm) and height ($h = 150$
5 μm or $[2(150 \mu\text{m})+12 \mu\text{m}]$ for one- and two-paper layers respectively), while indirectly proportional to
6 the channel length ($L = 11.2 \mu\text{m}$) and the solution viscosity. The fabrication scheme for a quasi-steady
7 flow device that was characterized for flow rate based on the change in fluid area within the device with
8 time is shown in Scheme 1. Similarly, Figures 1B and C show photographs of the wetting and the
9 normalized wetting area as a function of time. A steady increase in area with time is observed for both
10 one and two-layer devices. Assuming that a given change in area corresponds to a set volume of
11 solution flowing through the channel (i.e. assuming constant h throughout the device), a linear increase
12 in area within the wicking fan corresponds to a steady flow of solution through the channel. The use of
13 two layers of paper increased the flow rate by 273% compared to a single layer device. As discussed
14 previously, the increase in flow rate for the two-layer relative to the one-layer device is due to the gap
15 present between paper layers and therefore larger capillary height. Although initial flow through the
16 channel is not steady, once the fluid front reaches the fan region, a steady flow rate is maintained. This
17 was therefore used as a starting point for carrying out analytical measurements.
18
19
20

21
22 To the best of our knowledge this is the first time change in fluid area within a paper-based device has
23 been used to characterize flow rate through a sample inlet. Previous work has measured the rate a dye
24 fluid front moves through a pre-wetted channel.³⁷ However, this method can only monitor the dye
25 speed through the length of the channel, and cannot measure flow rate once the dye reaches the
26 wicking pad. Another method made use of alternating the sample inlet between solutions with or
27 without dye to form bands of dye.²⁹ The flow rate was then determined based on the speed the bands
28 moved through the channel with time. While this method worked well for a slow flow rate material such
29 as nitrocellulose, the method required precise changing of solutions to form the bands, which do not
30 have time to form within the inlet channel in faster flow rate materials such as the Whatman Grade 1
31 filter paper used in this study. An alternative study measured the change in radius and, therefore,
32 change in volume of imbibed solution within a hemispherical-glass matrix from a point source.³⁸ The
33 study also determined that radial change in volume was constant with time, matching well with our
34 results for a thin membrane change in area. Our presented method, therefore, serves as a more
35 universal and simple means for monitoring flow rate through a sample inlet within paper devices,
36 especially in device geometries that deviate from Lucas-Washburn behavior.
37
38
39

40 **Microwire ePAD Electrochemical Behavior with Flow.** Electrochemical detection in ePADs is usually
41 carried out in quiescent solution and as such, detection under steady flow conditions has not been
42 studied extensively in paper. A comparison to electrochemical detection at Au microwire electrodes
43 with and without flow in ePADs was carried out using LSV in 5 mM $\text{K}_4\text{Fe}(\text{CN})_6/\text{K}_3\text{Fe}(\text{CN})_6$ in 0.5 M KCl.
44 Figure 2A shows distinctive voltammograms indicative of mass-transport and diffusion limited currents
45 with flow and quiescent solution conditions, respectively. Unlike the peak-current behavior obtained for
46 the quiescent solution, a sigmoidal steady-state current is obtained within the flow device due to added
47 convection of analyte to the electrode surface. The measured LSVs showed a peak current increase from
48 3.77 ± 0.58 for one-layer devices in the absence of flow, to $12.17 \pm 0.71 \mu\text{A}$ with the addition of flow. For
49 two-layer devices, peak current increased from $5.92 \pm 0.81 \mu\text{A}$ to $20.66 \pm 0.32 \mu\text{A}$ with the addition of
50 flow. The slightly larger increase in peak current with flow addition for a two-layer device (249 %
51 increase) when compared with a one-layer device (222 % increase) is probably due to a further swelling
52 of the gap between the layers of paper with flow that cannot occur in a one-layer device, as the
53 electrode is held more tightly in place with packing tape. The slightly larger increase in peak current
54 from one- to two-layers with (69.7% increase) and without flow (56.9% increase) is also indicative of the
55 increase in gap-height that acts a larger capillary with flow. The optimal device design incorporated
56
57
58
59
60

sandwiching of the electrodes between two layers of paper (Figure 2B) in order to maximize the electrode surface area and flow rate of species to the electrode surface.

Figure 3A shows the amperometric current response of the device with no flow and the subsequent spike and plateau of current from the flow of solution across the electrodes, due to droplet addition to the well inlet. Addition of the droplet to the device creates an increase in current due to an increase in mass-transport. Because of the perturbation of the double layer with flow, a small spike can be seen at the start of flow, immediately after droplet addition. The spike decays while the flow rate stabilizes, reaching a plateau current. During the plateau, steady-flow behavior is maintained and an average current measurement is recorded. This plateau current is dependent on both the flow rate and the amount of faradaic and non-faradaic current being passed (Figure 3B). The plateau is followed by a decay of signal back to the baseline when flow stops due to liquid depletion at the inlet. While the initial increase in current is rapid as the droplet fills the already wet capillary network and flows through, the decay follows a more gradual decrease. Microscopy of flow through paper shows that this more gradual decrease is due to the capillary force at the fluid front having to break the surface tension of filled pores in the paper to remove solution.

The device repeatability under steady-flow was determined through repeated injections of a blank (0.5 M KCl) or a sample (5 mM $K_4Fe(CN)_6/K_3Fe(CN)_6$ in 0.5 M KCl). An example amperogram is shown in Supplemental Figure S2. The plateau current without faradaic reactions occurring created a small change in cathodic background current (no flow) of -4.9 ± 0.5 nA ($n = 11$) when blank 5 μ L injections were added (Supplemental Figure S3B). The average combined cathodic faradaic and non-faradaic current was measured to be $-6.66 \mu A \pm 0.22 \mu A$ ($n = 16$ injections) at the plateau from the sample flow across the electrode with repeated 5 μ L injections. However, an interesting phenomenon occurred when doing anodic detection (Supplemental Figure S3A). A smaller overall current response was measured from both blank (1.69 ± 0.27 nA ($n = 11$)) and sample ($-1.97 \mu A \pm 0.14 \mu A$ ($n = 10$)) injections. This behavior was seen for both Au and Pt working electrodes and for different species detected ($K_4Fe(CN)_6$ and HQ). While the cause of this phenomenon is unclear, the device still behaved consistently with repeated injections for oxidation. This could possibly be due to some interaction of the electrode with the cellulose matrix. Cellulose is a polysaccharide comprised of glucose, which has been found to adsorb to both gold and platinum surfaces from near neutral (pH 7.4) to more basic solutions.^{39,40} This phenomenon could explain the initial decline in current, due to a decrease in active sites for electrochemical detection that then stabilizes after an absorption layer is formed.

Microwire ePAD Calibration. Next, the ePAD was used for the detection of $K_4Fe(CN)_6/K_3Fe(CN)_6$ and HQ/BQ as model inner sphere inorganic and organic redox species. Figure 3C shows the resulting calibration plots from several devices ($n = 13$) with good linearity and correlation ($R^2 \geq 0.998$). The slopes also correlate with increasing electron-transfer processes, where the slope approximately doubles when going from $K_4Fe(CN)_6/K_3Fe(CN)_6$ (slope = $2.834 \mu A / \mu M$, 1 electron process) to HQ/BQ (slope = $6.389 \mu A / \mu M$, 2 electron process). While good reproducibility was found within flow devices, average measurements between devices however, could produce RSDs that were greater than desired, as seen in Supplemental Figure S4A, where average RSDs were 10.65%. As each sensor is assembled by hand and sometimes by different individuals, this was attributed to small differences in fabrication, such as the amount of pressure used to seal the device or variations in alignment. One way to account for device-to-device variations is to normalize the signal using a standard solution addition (Supplemental Figure S4B), which reduced average RSDs to 4.56%. Calibration plots for both oxidation and reduction of $K_4Fe(CN)_6/K_3Fe(CN)_6$ at both Au and Pt electrodes still show good linearity ($R^2 \geq 0.998$) with average RSD of 7.46% (Supplemental Figure S5). It is of interest to note that all of the slopes are nearly equivalent

1
2
3 with oxidation and reduction slope values of 0.1983 mM^{-1} and 0.2031 mM^{-1} at Au and 0.2001 mM^{-1} and
4 0.1983 mM^{-1} at Pt microwire electrodes when each device is normalized to the same 5 mM standard
5 injection. The same slopes are also nearly equivalent to each other when more than one wire is used to
6 form the working electrode (Supplemental Figure S6). Supplemental Figure S6B shows the effect
7 doubling the electrode area has on the measured slope, 1.882 for one-wire to $2.95 \text{ } \mu\text{A}/\text{mM}$ for a two-
8 wire working electrode device. These differences in electrode area were normalized when using a
9 standard, however, and both one-wire (normalized slope = 0.1998 mM^{-1}) and two-wire (normalized
10 slope = 0.1871 mM^{-1}) working electrodes produced similar normalized slopes (Supplemental Figure S6C).
11 The two-wire slope in Supplemental Figure S6C is probably slightly lower than one-wire due to an
12 increase in background current determined when using a working potential $> \pm 0.5 \text{ V}$ vs Au or Pt pseudo
13 reference electrodes for both Au and Pt working electrodes respectively (Supplemental Figure S7).
14 Lower applied potentials resulted in lower background signal and the use of two working electrodes
15 resulted in greater current that could be more easily measured by the potentiostat.
16
17
18

19 **Enzymatic Detection.** As proof of concept, the quasi-steady flow device was implemented for the
20 continuous monitoring of enzymatic activity. Enzymatic assays have been widely used as analytical
21 detection methods due to their selectivity and sensitivity to target analytes. Examples of these assays
22 include; clinical assays where enzymes react with target health indicators to produce a detectable
23 product,⁴¹ as detectable tags in enzyme-linked immunosorbent assays (ELISAs),⁴² as an indicator of gene
24 expression via the production or deletion of specific genes for enzyme production,⁴³ and in bacterial
25 assays where the presence of bacterially produced enzymes is used to identify bacterial species.⁴⁴ β -
26 galactosidase is commonly used as a tag in ELISAs, a reporter marker in gene expression, and as a
27 bacterial indicator for total coliform counts and *E. coli* species identification.⁴⁵ β -galactosidase
28 hydrolyzes the β -glycosidic bond between a galactose and its organic moiety and its enzyme activity is
29 then measured via product formation. The steady-flow device was used to measure the activity of β -
30 galactosidase via the production of p-aminophenol (PAP) from the substrate p-aminophenyl-
31 galactopyranoside (PAPG) (Figure 4A). PAP is electrochemically active; and thus detectable through a
32 two electron oxidation reaction. Its use for the electrochemical detection of enzymatic activity has been
33 previously well described.⁴⁶ As shown in Figure 4B, both the substrate PAPG and product PAP are
34 electrochemically active with peak potentials at 0.45 and 0.15 V vs Pt respectively, and an optimal
35 amperometric over-potential was determined to be 0.3 V vs Pt (Figure 4C). PAP calibration was then
36 determined using flow devices with dual microwire Pt working electrodes at 0.3 V (Supplemental Figure
37 S8), and a $31 \text{ } \mu\text{M}$ limit of detection was calculated (mean + 3 SD).
38
39
40
41
42

43 The enzyme kinetics of β -galactosidase for the electrochemical reaction were studied amperometrically
44 at 0.3 V vs Pt by continuously adding the reaction solution (varying PAPG concentration with $10 \text{ U}/\text{mL}$
45 enzyme in PBS) to the device and monitoring the changes in plateau current with time. Once the
46 measured current was converted to PAP concentration using a calibration curve, the reaction rate could
47 be obtained and plotted against the starting substrate concentration (Figure 5A). Figure 5A is a
48 Michaelis-Menten plot showing the rate of reaction beginning to plateau above 1 mM PAPG, indicating a
49 saturation in the catalytic capability of the enzyme in solution.⁴⁷
50
51

52 The Lineweaver-Burk plot in Figure 5B serves as a useful graphical representation, whereby the
53 maximum rate of reaction (V_{max}) and Michaelis-Menten constant (K_m) can be easily calculated from the
54 y-intercept ($1/V_{max}$) and slope (K_m/V_{max}) or x-intercept ($-1/K_m$), from experimentally determined
55 changes in rate (V) measured from using different concentrations of substrate ($[S]$).³⁴ The V_{max} and K_m
56 values were experimentally determined to be $0.079 \text{ mM}/\text{min}$ and 0.36 mM respectively. An enzyme
57 turnover number (k_{cat}), which is the maximum number of substrate molecules turned over by an
58
59
60

1
2
3 enzyme molecule per second, was calculated from the determined V_{max} to be 94 s^{-1} . A separate study in
4 quiescent solution by Laczka *et al.* using a Au microelectrode array as the working electrode for the
5 electrochemical detection of PAP, found a similar K_m value of 0.43 mM, which indicates a similar
6 substrate affinity when reacting PAPG with β -galactosidase.⁴⁸ For the same reaction, Viratelle *et al.* also
7 found similar K_m (0.33 mM) and k_{cat} (90 s^{-1}) values using a spectrophotometer at 306 nm for PAP
8 detection.⁴⁹ The similarities of our calculated values to literature, for more complex or expensive
9 detection platforms, indicate that the proposed disposable and simple to fabricate device provides a
10 viable and alternative analytical method for detecting enzyme kinetics in real time.
11
12

13
14 It is also plausible to utilize the quasi-steady flow device to perform immunoassays including ELISAs by
15 depositing biorecognition elements capable of generating electrochemical signals upon binding to target
16 analyte on the surface of the working electrode. This device could use target binding antibodies, for
17 example, attached to the microwire working electrode or the paper itself. Similar to a lateral flow assay
18 (LFA), reagents can be stored within the device and upon addition of sample, analyte can be reacted,
19 captured, and washed of unbound material prior to electrochemical product formation detection at the
20 microwire electrodes. Detection of a dengue biomarker in a lateral flow assay has been previously
21 demonstrated by Sinawang *et al.* using an antibody-conjugated screen-printed gold electrode at which
22 the analyte was captured and later sandwiched with a secondary antibody labeled with ferrocene.⁵⁰
23 Platinum electrodes have also been employed to carry out ELISA in a flow-based system for detecting
24 cortisol.⁵¹ In electrochemical ELISAs, enzymes are often conjugated to a secondary antibody to convert
25 the substrate into a redox active species product.⁵¹⁻⁵³
26
27
28
29
30
31

32 Conclusions

33
34 The use of a steadily increasing capillary network, to generate quasi-steady flow, has been studied for
35 the first time in ePADs. The device is simple and inexpensive to fabricate, and has been employed for
36 electrochemical detection at microwire electrodes. The use of single- and double-paper layers can be
37 used to control flow rate by changing the effective pore radius of the device. The resulting increase in
38 fluid transfer through the device when two-layers of paper are used is achieved by incorporating the gap
39 between the layers of paper that acts as a larger capillary. Both colorimetric and electrochemical
40 detection within the device, using image processing software and microwire electrodes respectively,
41 provided reproducible results and can be used in future device development to monitor flow response
42 within paper-based devices. Additionally, calibration plots normalized to a standard provided improved
43 measurement reproducibility between devices. Future device design could incorporate a separate layer
44 with stored standard reagents that could be measured at the end of the device use for normalization
45 purposes. As proof-of-concept, the devices were used to measure enzyme activity for β -galactosidase
46 and PAP, which provided kinetic values similar to those found in the literature, demonstrating the
47 usefulness of this device. Moreover, this device design could incorporate modified microwire electrodes
48 to improve detection sensitivity or to capture species from solution at the electrode surface while
49 utilizing device flow. This ePAD, therefore, serves as an alternative detection platform to current
50 colorimetric methods and as a faster analysis approach for measuring a set volume of solution in
51 laboratory tests such as lateral flow assays.
52
53
54
55

56 Acknowledgements

This work was partially supported the National Institutes of Health (ES023496). Additional support was received from Colorado State University. The authors also thank Robert Channon for editorial assistance.

Associated Content

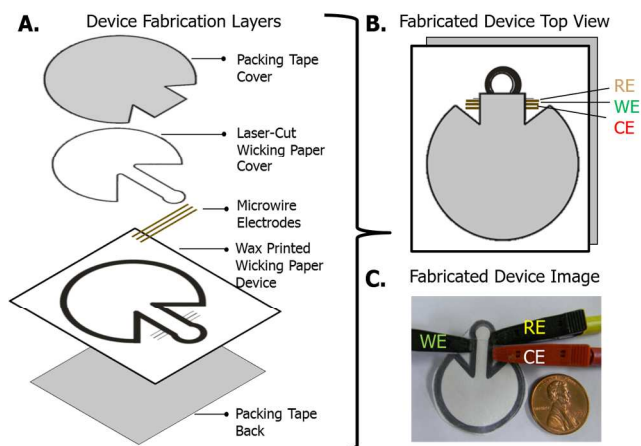
Supporting Information: Details of device flow characterization, pore radius determination, electrochemical measurements, repetitive signal response, and calibration.

References

- (1) Rackus, D. G.; Shamsi, M. H.; Wheeler, A. R. *Chemical Society Reviews* **2015**, *44*, 5320-5340.
- (2) Volpatti, L. R.; Yetisen, A. K. *Trends in Biotechnology* **2014**, *32*, 347-350.
- (3) Martinez, A. W.; Phillips, S. T.; Butte, M. J.; Whitesides, G. M. *Angewandte Chemie-International Edition* **2007**, *46*, 1318-1320.
- (4) Cate, D. M.; Adkins, J. A.; Mettakoonpitak, J.; Henry, C. S. *Analytical Chemistry* **2015**, *87*, 19-41.
- (5) Nery, E. W.; Kubota, L. T. *Anal Bioanal Chem* **2013**, *405*, 7573-7595.
- (6) Yetisen, A. K.; Akram, M. S.; Lowe, C. R. *Lab Chip* **2013**, *13*, 2210.
- (7) Fridley, G. E.; Le, H. Q.; Fu, E.; Yager, P. *Lab Chip* **2012**, *12*, 4321-4327.
- (8) Carrilho, E.; Martinez, A. W.; Whitesides, G. M. *Analytical Chemistry* **2009**, *81*, 7091-7095.
- (9) Meredith, N. A.; Quinn, C.; Cate, D. M.; Reilly, T. H.; Volckens, J.; Henry, C. S. *Analyst* **2016**, *141*, 1874-1887.
- (10) Lisowski, P.; Zarzycki, P. K. *Chromatographia* **2013**, *76*, 1201-1214.
- (11) Dungchai, W.; Chailapakul, O.; Henry, C. S. *Analytical Chemistry* **2009**, *81*, 5821-5826.
- (12) Rattanarat, P.; Dungchai, W.; Cate, D.; Volckens, J.; Chailapakul, O.; Henry, C. S. *Analytical Chemistry* **2014**, *86*, 3555-3562.
- (13) Nie, Z.; Deiss, F.; Liu, X.; Akbulut, O.; Whitesides, G. M. *Lab on a Chip* **2010**, *10*, 3163-3169.
- (14) Carvalhal, R. F.; Simão Kfour, M.; de Oliveira Piazzetta, M. H.; Gobbi, A. L.; Kubota, L. T. *Analytical Chemistry* **2010**, *82*, 1162-1165.
- (15) Lankelma, J.; Nie, Z.; Carrilho, E.; Whitesides, G. M. *Anal Chem* **2012**, *84*, 4147-4152.
- (16) Renault, C.; Anderson, M. J.; Crooks, R. M. *Journal of the American Chemical Society* **2014**, *136*, 4616-4623.
- (17) Dossi, N.; Toniolo, R.; Pizzariello, A.; Impellizzeri, F.; Piccin, E.; Bontempelli, G. *ELECTROPHORESIS* **2013**, n/a-n/a.
- (18) Adkins, J.; Boehle, K.; Henry, C. *ELECTROPHORESIS* **2015**, *36*, 1811-1824.
- (19) Mettakoonpitak, J.; Boehle, K.; Nantaphol, S.; Teengam, P.; Adkins, J. A.; Srisa-Art, M.; Henry, C. S. *Electroanalysis* **2016**, DOI: 10.1002/elan.201501143.
- (20) Nie, Z.; Nijhuis, C. A.; Gong, J.; Chen, X.; Kumachev, A.; Martinez, A. W.; Narovlyansky, M.; Whitesides, G. M. *Lab on a Chip* **2010**, *10*, 477-483.
- (21) Siegel, A. C.; Phillips, S. T.; Dickey, M. D.; Lu, N.; Suo, Z.; Whitesides, G. M. *Advanced Functional Materials* **2010**, *20*, 28-35.
- (22) Cunningham, J. C.; Brenes, N. J.; Crooks, R. M. *Analytical Chemistry* **2014**, *86*, 6166-6170.
- (23) Ge, L.; Wang, S.; Yu, J.; Li, N.; Ge, S.; Yan, M. *Advanced Functional Materials* **2013**, *23*, 3115-3123.
- (24) Hu, C.; Bai, X.; Wang, Y.; Jin, W.; Zhang, X.; Hu, S. *Analytical Chemistry* **2012**, *84*, 3745-3750.
- (25) García, C. D.; Henry, C. S. *Analytical Chemistry* **2003**, *75*, 4778-4783.
- (26) Fosdick, S. E.; Anderson, M. J.; Renault, C.; DeGregory, P. R.; Loussaert, J. A.; Crooks, R. M. *Analytical Chemistry* **2014**, *86*, 3659-3666.

- 1
2
3
4 (27) Adkins, J. A.; Henry, C. S. In *International Conference on Miniaturized Systems for Chemistry and Life*
5 *Sciences*; RSC Publishing: San Antonio, TX, 2014, pp 1583-1585.
- 6 (28) Adkins, J. A.; Henry, C. S. *Analytica Chimica Acta* **2015**, *891*, 247-254.
- 7 (29) Mendez, S.; Fenton, E. M.; Gallegos, G. R.; Petsev, D. N.; Sibbett, S. S.; Stone, H. A.; Zhang, Y.; López,
8 G. P. *Langmuir* **2009**, *26*, 1380-1385.
- 9 (30) Li, K.; Zhang, D.; Bian, H.; Meng, C.; Yang, Y. *Scientific Reports* **2015**, *5*, 14085.
- 10 (31) Washburn, E. W. *Physical Review* **1921**, *17*, 273-283.
- 11 (32) Lucas, R. *Kolloid-Z.* **1918**, *23*.
- 12 (33) Lin, T.; Li, Z.; Song, Z.; Chen, H.; Guo, L.; Fu, F.; Wu, Z. *Talanta* **2016**, *148*, 62-68.
- 13 (34) Lineweaver, H.; Burk, D. *Journal of the American Chemical Society* **1934**, *56*, 658-666.
- 14 (35) Camplisson, C. K.; Schilling, K. M.; Pedrotti, W. L.; Stone, H. A.; Martinez, A. W. *Lab on a Chip* **2015**,
15 *15*, 4461-4466.
- 16 (36) Fu, E.; Ramsey, S.; Kauffman, P.; Lutz, B.; Yager, P. *Microfluid Nanofluid* **2011**, *10*, 29-35.
- 17 (37) Lee, J.-H.; Chang, C.-K.; Park, J. In *International Conference on Miniaturized Systems for Chemistry*
18 *and Life Sciences*; RSC Publishing: Gyeongju, KOREA, 2015, pp 1338-1340.
- 19 (38) Xiao, J.; Stone, H. A.; Attinger, D. *Langmuir* **2012**, *28*, 4208-4212.
- 20 (39) Yan, X.; Ge, X.; Cui, S. *Nanoscale Research Letters* **2011**, *6*, 313-313.
- 21 (40) Pasta, M.; La Mantia, F.; Cui, Y. *Electrochimica Acta* **2010**, *55*, 5561-5568.
- 22 (41) Hemalatha, T.; UmaMaheswari, T.; Krithiga, G.; Sankaranarayanan, P.; Puvanakrishnan, R. **2013**.
- 23 (42) Lequin, R. M. *Clinical chemistry* **2005**, *51*, 2415-2418.
- 24 (43) Gallagher, S. R. *GUS protocols: using the GUS gene as a reporter of gene expression*; Academic Press,
25 2012.
- 26 (44) Batt, C. A. *Encyclopedia of Food Microbiology*, 2nd ed.; Academic Press: Oxford, 2014.
- 27 (45) Husain, Q. *Critical Reviews in Biotechnology* **2010**, *30*, 41-62.
- 28 (46) Tang, H. T.; Lunte, C. E.; Halsall, H. B.; Heineman, W. R. *Analytica Chimica Acta* **1988**, *214*, 187-195.
- 29 (47) Johnson, K. A.; Goody, R. S. *Biochemistry* **2011**, *50*, 8264-8269.
- 30 (48) Laczka, O.; Ferraz, R. M.; Ferrer-Miralles, N.; Villaverde, A.; Muñoz, F. X.; Campo, F. J. d. *Analytica*
31 *Chimica Acta* **2009**, *641*, 1-6.
- 32 (49) Viratelle, O. M.; Yon, J. M. *European Journal of Biochemistry* **1973**, *33*, 110-116.
- 33 (50) Sinawang, P. D.; Rai, V.; Ionescu, R. E.; Marks, R. S. *Biosens. Bioelectron.* **2016**, *77*, 400-408.
- 34 (51) Yamaguchi, M.; Matsuda, Y.; Sasaki, S.; Sasaki, M.; Kadoma, Y.; Imai, Y.; Niwa, D.; Shetty, V. *Biosens.*
35 *Bioelectron.* **2013**, *41*, 186-191.
- 36 (52) Akanda, M. R.; Joung, H.-A.; Tamilavan, V.; Park, S.; Kim, S.; Hyun, M. H.; Kim, M.-G.; Yang, H.
37 *Analyst* **2014**, *139* (6), 1420-1425.
- 38 (53) Bhimji, A.; Zaragoza, A. A.; Live, L. S.; Kelley, S. O. *Anal. Chem.* **2013**, *85* (14), 6813-6819.
- 39
40
41
42
43
44
45
46
47
48
49
50
51
52
53
54
55
56
57
58
59
60

Figures



Scheme 1. Quasi-stationary flow ePAD fabrication showing (A) the device layers, (B) the top view of the device design (with packing tape back layer moved to the side slightly for visualization), and (C) the device image with electrode leads attached.

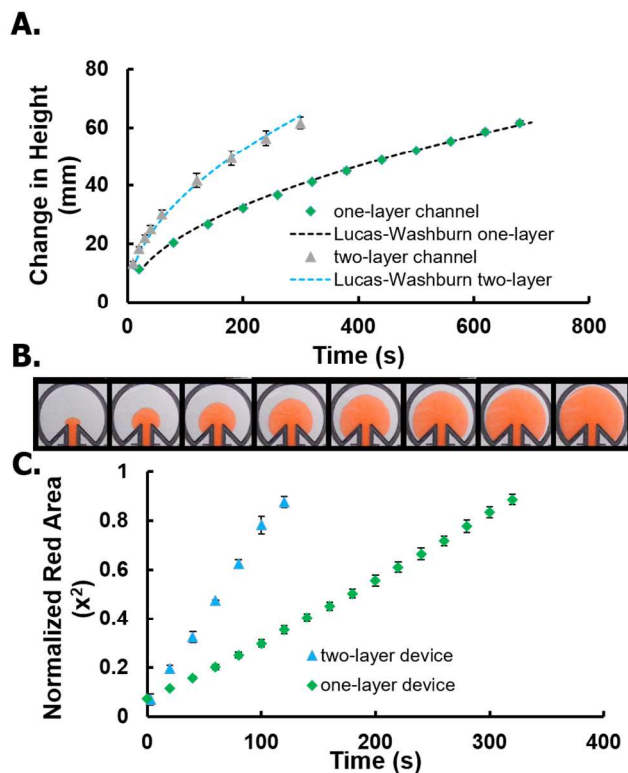


Figure 1. Flow rate characterization for (A) straight channels and (B and C) quasi-steady flow devices with either one- or two-layers of paper. (A) Straight channel flow behavior is determined experimentally and modeled using (Eq. 1). (B) Quasi-stationary flow device images were taken every 20 s, and (C) flow rate was calculated from these images *via* change in red area within the device and normalized to the total device area. Time 0 s = time solution reaches the end of the channel for start of the steady flow regime. (n=4 devices/measurement)

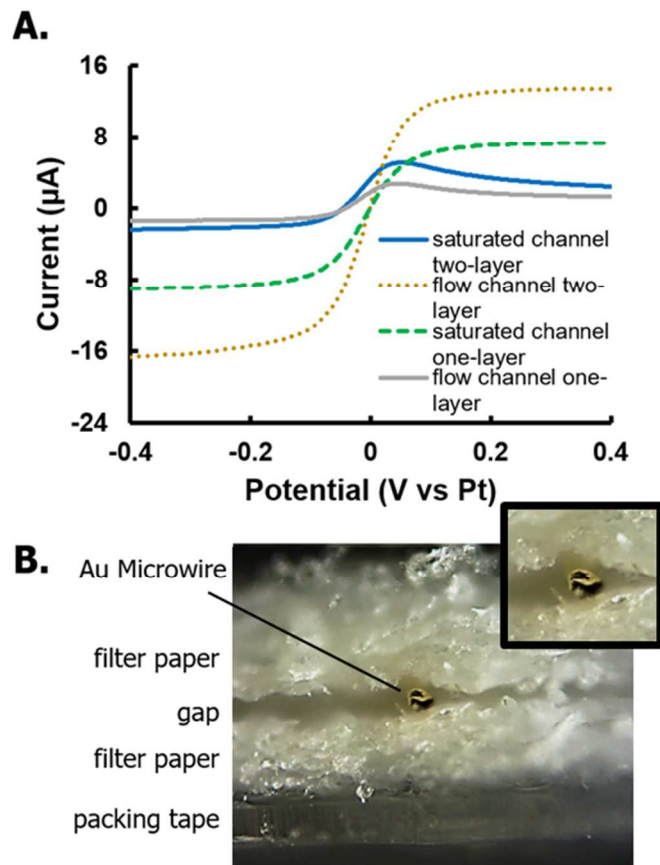


Figure 2. Electrochemical detection showing (A) the LSV current profiles for one- and two- layer devices either with quasi-steady flow or without flow in a saturated channel using 5 mM $K_4Fe(CN)_6/K_3Fe(CN)_6$ in 0.5 M KCl, detected at a 25 μm diameter Au microwire electrodes (Pt counter and reference). (B) Image of channel cross-section, cut down the center, showing a 25 μm Au electrode sandwiched between two paper layers with an enlarged inset of the cut, circular end of the Au microwire electrode in the upper right corner.

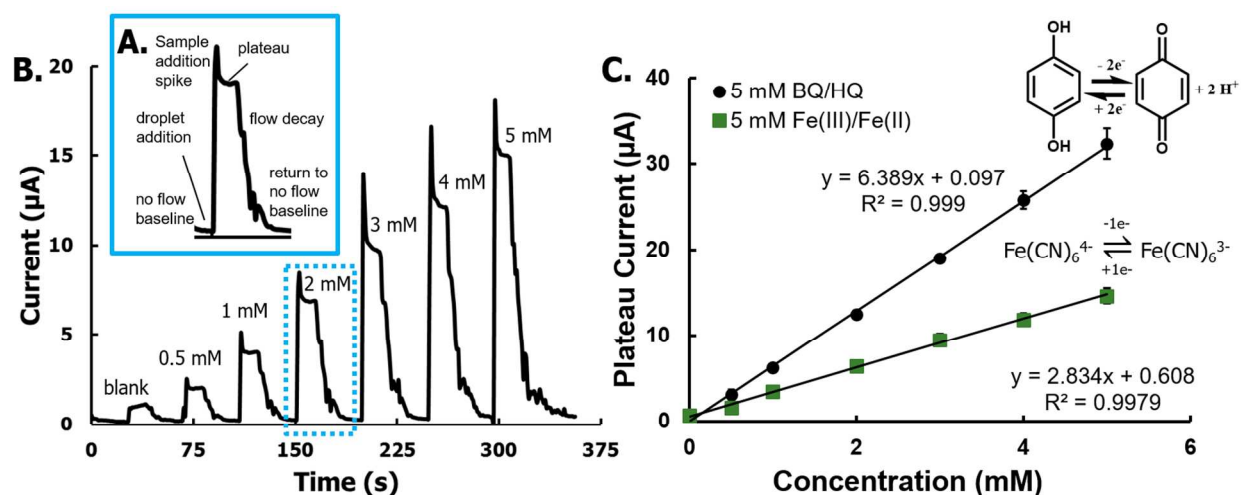


Figure 3. Quasi-stationary flow ePAD amperometric detection showing (A) the detailed flow-current profile blown up from the 2 mM injection of (B) the full calibration amperometric profile for increasing concentrations of $\text{K}_4\text{Fe}(\text{CN})_6/\text{K}_3\text{Fe}(\text{CN})_6$ in 0.5 M KCl and (C) plotted as the average peak plateau current in the calibration plots for increasing concentrations of $\text{K}_4\text{Fe}(\text{CN})_6/\text{K}_3\text{Fe}(\text{CN})_6$ ($n=9$ device) or HQ and BQ ($n=4$ devices) in 0.5 M KCl detected at 25- μm diameter gold microwire electrodes at -600 mV.

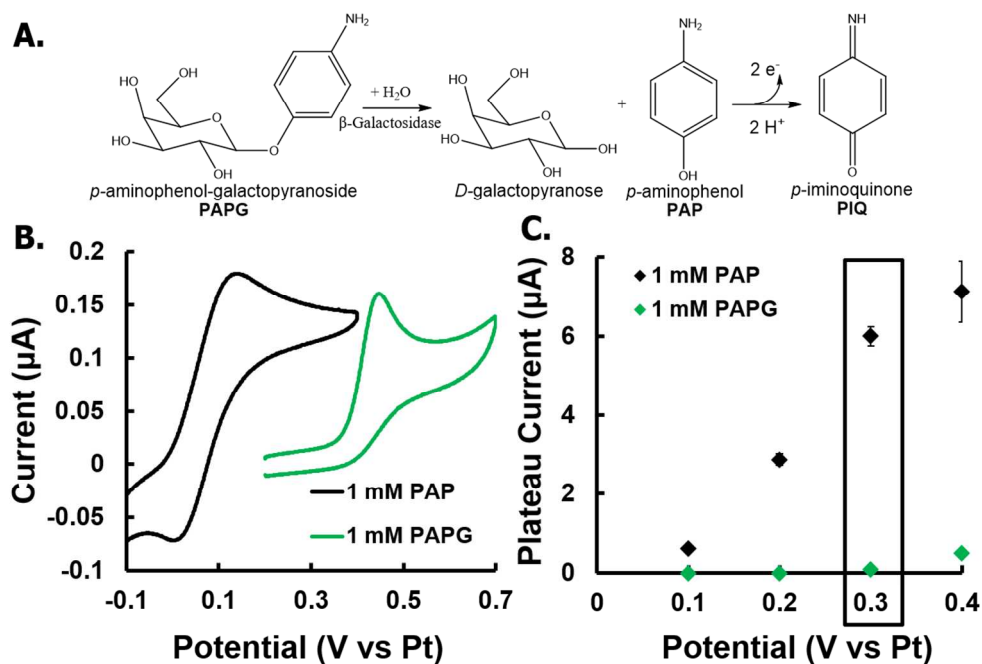


Figure 4. Optimal potential determination of PAP formed from (A) the reaction of PAPG with β -galactosidase and detected electrochemically through a $2e^-$ oxidation reaction. (B) Cyclic voltammograms of 1 mM PAP or PAPG in pH 7.4 PBS buffer were measured using Pt microwire electrodes in saturated paper-based channel devices without flow and (C) the resulting hydrodynamic voltammograms using amperometric detection with flow ($n=4$). The optimal potential for amperometric detection is designated at 0.3 V.

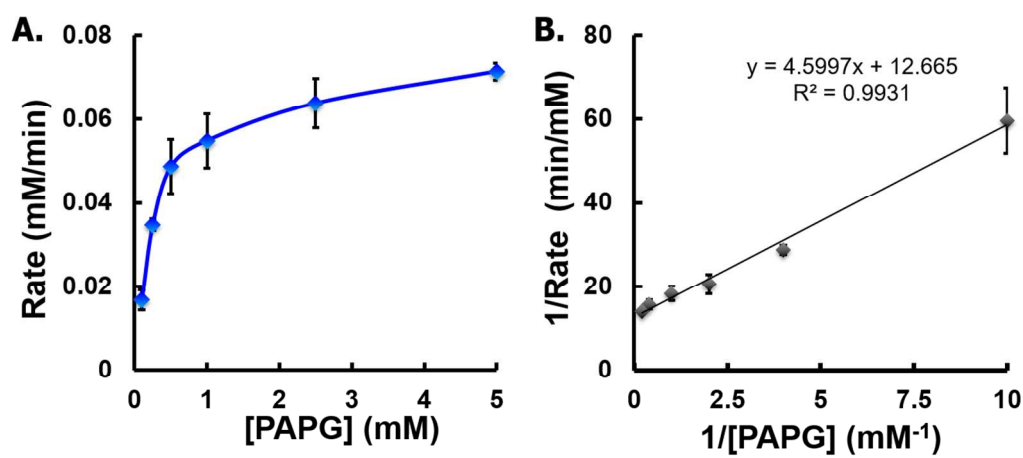
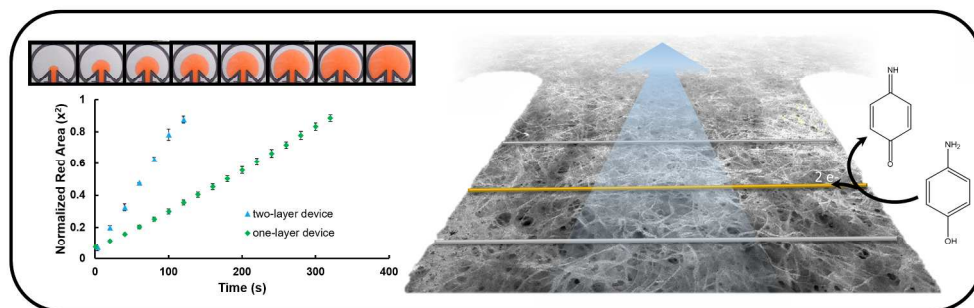


Figure 5. Enzyme kinetics plots determined by measuring β -galactosidase reaction with PAPG to form PAP in (A) Michaelis-Menten (B) Lineweaver-Burk plots (n=4)



693x228mm (96 x 96 DPI)